Korean J. Chem. Eng., 32(2), 206-215 (2015)
DOI: 10.1007/s11814-014-0186-0

pISSN: 0256-1115
eISSN: 1975-7220

Quaternary $Pt_2Ru_1Fe_1M_1/C$ (M=Ni, Mo, or W) catalysts for methanol electro-oxidation reaction

Min Ku Jeon*,†, Ki Rak Lee*, Hyung Joon Jeon, Paul J. McGinn***, Kweon Ho Kang*, and Geun Il Park***

*Nuclear Fuel Cycle Process Development Division, Korea Atomic Energy Research Institute, Daedeok-daero 989-111, Yuseong-gu, Daejeon 305-353, Korea
**Institute for Integrated Cell-Material Sciences (iCeMS), Kyoto University, Katsura, Nishikyo-ku, Kyoto 615-8510, Japan
***Department of Chemical and Biomolecular Engineering, University of Notre Dame, Notre Dame, IN 46556, USA
(*Received 4 March 2014 • accepted 1 July 2014*)

Abstract−Quaternary $Pt_2Ru_1Fe_1M_1/C$ (M=Ni, Mo, or W) catalysts were investigated for the methanol electro-oxidation reaction (MOR). Electrocatalytic activities of the quaternary catalysts for CO electro-oxidation were studied via CO stripping experiments, and the $Pt_2Ru_1Fe_1Ni_1/C$ and $Pt_2Ru_1Fe_1W_1/C$ catalysts exhibited lowered on-set potential compared to that of a commercial PtRu/C catalyst. MOR activities of the quaternary catalysts were determined by linear sweep voltammetry (LSV) experiments, and the $Pt_2Ru_1Fe_1W_1/C$ catalyst outperformed the commercial PtRu/C catalyst by 170 and 150% for the mass and specific activities, respectively. X-ray photoelectron spectroscopy (XPS) was employed to analyze surface oxidation states of constituent atoms, and it was identified that the structure of the synthesized catalysts are close to a nano-composite of Pt and constituent metal hydroxides and oxides. In addition, the XPS results suggested that the bi-functional mechanism accounts for the improved performance of the $Pt_2Ru_1Fe_1Ni_1/C$ and Pt_2Ru_1 Fe_1W_1/C catalysts.

Keywords: Methanol Electro-oxidation Reaction, Direct Methanol Fuel Cell, Electrocatalyst, X-ray Photoelectron Spectroscopy, CO Electro-oxidation

INTRODUCTION

Development of high performing methanol electro-oxidation reaction (MOR) electrocatalysts is desired due to their use in direct methanol fuel cells (DMFCs). DMFC has the attractive characteristic that it uses a liquid fuel, enabling design and fabrication of small cells. However, the use of methanol also has some drawbacks, such as low catalytic activity for the MOR and methanol cross-over from the anode to the cathode, resulting in suppressed cathode performance [1]. Pure platinum was first introduced for the MOR, but CO poisoning caused a rapid drop of catalytic activity. The poor CO tolerance of pure Pt catalyst was significantly improved by incorporating Ru, and a bi-functional mechanism was suggested to account for the improved CO tolerance [2-5]. According to the bi-functional mechanism, CO produced on the Pt surface reacts with OH generated on the surface of Ru to produce CO_2. The following reactions explain the bi-functional mechanism:

$$Pt+CH_3OH \rightarrow Pt\text{-}CO+4H^++4e^- \quad (1)$$

$$Ru+H_2O \rightarrow Ru\text{-}OH+H^++e^- \quad (2)$$

$$Pt\text{-}CO+Ru\text{-}OH \rightarrow Pt+Ru+CO_2+H^++e^- \quad (3)$$

Although the PtRu catalyst achieved significantly improved MOR activity, research continues in the quest for catalysts with higher activity, lower cost, and enhanced stability. Among various efforts to develop highly active MOR electrocatalysts, transition metal doped PtRu catalysts such as PtRuNi [6-9], PtRuCo [10,11], PtRuMo [12], and PtRuW [10,11,13-15] exhibited promising results [16-18]. In addition to the bi-functional effect, electronic effect also accounts for the improved MOR activity of the transition metal doped PtRu catalysts [19-22]. Briefly, the electronic effect suggests that a modification of the Pt electronic structure is induced by neighboring transition metals, resulting in weakened Pt-CO bonding. Normally, the bi-functional mechanism can be identified through CO stripping experiments, because a lowered on-set potential for the CO_{ads} electro-oxidation reaction is observable when the bi-functional mechanism is operative. On the other hand, X-ray photoelectron spectroscopy (XPS) is widely employed to verify the electronic effect, because a change of Pt electronic state is caused by the transition elements.

Previously, Jeon et al. [23] reported that $Pt_2Ru_1Fe_1/C$ catalyst (Pt RuFe/C) significantly outperformed a binary PtRu/C catalyst. The high activity of the PtRuFe/C catalyst was also observed in a combinatorial study of various compositions of this ternary system [24]. The XPS analysis results revealed that electronic structure of Pt was significantly changed by the incorporation of Fe, meaning the electronic effect of Fe could weaken Pt-CO bonding to enhance the MOR and CO electro-oxidation activities of the PtRuFe/C catalyst. In the present study, a further investigation of the PtRuFe/C catalyst was performed by adding secondary transition metals of Ni, Mo, and W to produce quaternary compositions of $Pt_2Ru_1Fe_1Ni_1/C$ (PtRuFeNi/C), $Pt_2Ru_1Fe_1Mo_1/C$ (PtRuFeMo/C), and $Pt_2Ru_1Fe_1W_1/$

†To whom correspondence should be addressed.
E-mail: minku@kaeri.re.kr

C (PtRuFeW/C). A review of Demirci [18] provided a rationale for selecting Mo and W as additional members of the PtRuFe/C catalyst. In the review, Demirci suggests Mo and W as promising candidates to promote the MOR activity of the PtRu catalyst according to surface segregation and *d*-band shift properties. Nickel was chosen according to previous results which reported promising MOR activities of ternary Pt-Ru-Ni catalysts [6-9]. The quaternary composition electrocatalysts were analyzed using various techniques including X-ray diffraction (XRD), CO stripping, linear sweep voltammetry (LSV), and X-ray photoelectron spectroscopy (XPS).

EXPERIMENTAL

1. Synthesis of Catalysts

The quaternary catalysts were synthesized by a chemical reduction method using $NaBH_4$ as a reducer. First, the carbon support (Vulcan XC72R) was dispersed in an isopropyl alcohol and deionized (DI) water mixture. An appropriate amount of metal precursors was dissolved to adjust the atomic ratio of Pt : Ru : Fe : M (M=Ni, Mo, or W) to 2 : 1 : 1 : 1. The total amount of metals was adjusted to achieve 60 wt% metal loading. H_2PtCl_6, $RuCl_3$, $(NH_4)_2Fe(SO_4)_2$, $NiCl_2{\cdot}6H_2O$, $(NH_4)_6Mo_7O_{24}{\cdot}4H_2O$, and $(NH_4)_6H_2W_{12}O_{40}$ were employed as metal precursors. The mixture solution was stirred at 80 °C for 1 h, and then a 0.2 M $NaBH_4$ solution was added to the mixture for reduction of the precursors, followed by further stirring for 3 h at 80 °C to complete the reduction reaction. The reduced catalysts were filtered and washed with hot DI water and then dried at 120 °C for 12 h.

2. Structural and Electrochemical Characterization of the Catalysts

The XRD (Rigaku D/MAX-IIIC, 40 kV, 45 mA) patterns of the catalysts were measured at a scan rate of 3°/min in a θ-2θ scan mode. Electrochemical analysis was performed using a three-electrode-type beaker cell. Pt wire and Ag/AgCl electrodes (BAS Co., Ltd., MF-2052 RE-5B) were employed as the counter and reference electrodes, respectively. A glassy carbon electrode (3 mm dia., BAS Co. Ltd., MF-2012) was employed as a working electrode by depositing a catalyst layer on the electrode by the thin-film method [25]. A catalyst ink was prepared by sonicating a mixture of catalyst, DI-water, and 5 wt% Nafion ionomer solution to achieve homogeneous mixing. A quantity of the mixture was dripped onto the glassy carbon electrode and then solvent was removed at room temperature. After the solvent was evaporated, 5 wt% Nafion ionomer solution was dripped onto the catalyst layer to produce a Nafion thin-film on the catalyst layer to provide mechanical strength to the catalyst layer during electrochemical tests.

The CO stripping experiments were performed using 1 M $HClO_4$ solution as an electrolyte in a three-electrode-type beaker cell. Carbon monoxide was bubbled through the cell for 1 h while keeping the working electrode at 0.1 V (vs. reversible hydrogen electrode (RHE)) to saturate the catalyst surface with CO. Residual CO in the electrolyte solution was removed by purging nitrogen gas through the cell for 50 minutes. Carbon monoxide electro-oxidation was performed by increasing the potential of the working electrode from 0.1 to 1.2 V (vs. RHE) at a rate of 15 mV/s. When the potential reached 1.2 V (vs. RHE), the potential was cycled between 0.1 and 1.2 V at a scan rate of 15 mV/s to confirm complete removal of CO. MOR activities of the catalysts were measured by increasing the potential of the working electrode from 0.0 to 0.5 V at a ramping rate of 1 mV/s, which is so-called the LSV technique. All potentials in this paper were converted to the RHE scale.

The XPS experiments were performed using a surface analysis system (LHS-10, SPECS GmbH) equipped with a multiplate channel detector using Mg Kα radiation (8.4 kV and 14 mA). To measure the XPS spectra, the catalyst samples were pressed at 1,000 psi to fabricate a pellet. The pelletized samples were loaded into the preparation chamber and then transferred into the main chamber where the pressure was maintained at 1×10^{-9} Torr by using a turbo molecular pump.

RESULTS AND DISCUSSION

1. XRD Analysis Results

The XRD measurement results of the catalysts are shown in Fig. 1, with the peak positions of Pt for comparison purpose. Based on the (220) peak positions, signs of alloying were observed in the commercial PtRu/C (E-tek, 60 wt%, Pt : Ru=1 : 1 atomic ratio) and the quaternary catalysts. Lattice parameters of the samples could be calculated using an equation of

$$a(220)=\sqrt{2}\lambda_{K\alpha}/\sin\theta \tag{4}$$

where $\lambda_{K\alpha}$ represents wavelength of X-ray (0.15406 nm), and θ is

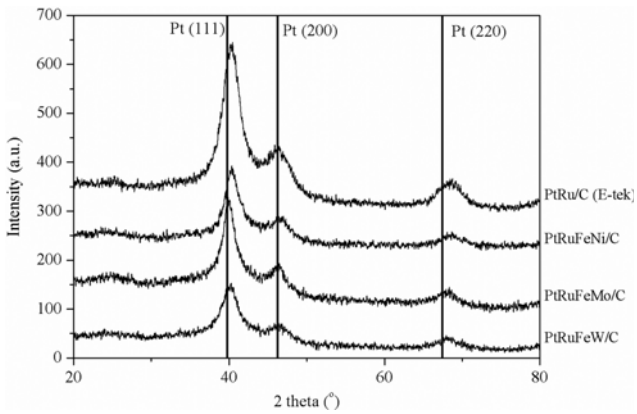

Fig. 1. The XRD patterns of the quaternary PtRuFeNi/C, PtRuFeMo/C, and PtRuFeW/C catalysts along with that of a commercial PtRu/C catalyst. Peak positions of pure platinum are denoted with solid vertical lines.

Table 1. Summary of the XRD measurement results

	(220) Peak position (°)	Lattice parameter (nm)	Degree of alloying	Crystallite size (nm)
PtRu/C	68.36	0.38904	0.202	2.7
PtRuFeNi/C	68.58	0.38845	0.237	3.0
PtRuFeMo/C	67.72	0.39080	0.084	3.0
PtRuFeW/C	68.10	0.38974	0.229	2.8

the angle at the peak maximum. The calculated lattice parameters are listed in Table 1. Degree of alloying values can be calculated by employing Vegard's law:

$$a_{alloy}=a_{Pt}-k\,x_m \quad (5)$$

where a_{alloy} is the lattice constant of alloy catalysts, a_{Pt}=0.39155 nm (the lattice parameter of pure carbon supported Pt), and k is a constant that represents the lattice parameter difference between Pt and Pt-M phases. In the present study, x_m is composed of three catalysts with identical atomic fraction; thus, the k values were calculated from average values of three metals for each catalyst. In other words, the following values were applied for the calculation of k values of the quaternary catalysts: 0.0124 nm for Ru [26], 0.01355 nm for Fe from $Pt_{0.5}Fe_{0.5}$ phase [27], 0.01345 nm for Ni from $Pt_{0.5}Ni_{0.5}$ phase [28], 0.0008 nm for Mo from $Pt_{0.8}Mo_{0.2}$ phase [29], and −0.00225 nm for W from $Pt_{0.5}W_{0.5}$ phase [30]. Thus, k values of the quaternary catalysts are 0.0131 nm for the PtRuFeNi/C catalyst, 0.0089 nm for the PtRuFeMo/C catalyst, and 0.0079 nm for PtRuFeMo/C catalyst, and calculated x_m values are listed in Table 1. Here, note that the degree of alloying values increased in the Ni and W incorporated catalysts, while it was significantly reduced in the PtRuFeMo/C catalyst. It is also interesting that the highest value of degree of alloying was only 0.237, suggesting that the catalysts might be composed of crystalline Pt-alloy nanoclusters with neighboring amorphous nano-particles of other constituent metals because only Pt peaks were identified in Fig. 1. Incomplete alloying of the catalysts reduced via chemical reagents ($NaBH_4$ in this study) or reduced at a low temperature was discussed in previous reports [31-33], and it was suggested that avoiding alloy formation is preferred for high MOR activity. Platinum crystallite sizes of the catalysts were determined by employing the Scherrer equation [34] on the width of (111) peak, giving results of 2.7, 3.0, 3.0, and 2.8 nm for the PtRu/C, PtRuFeNi/C, PtRuFeMo/C, and PtRuFeW/C catalysts, respectively.

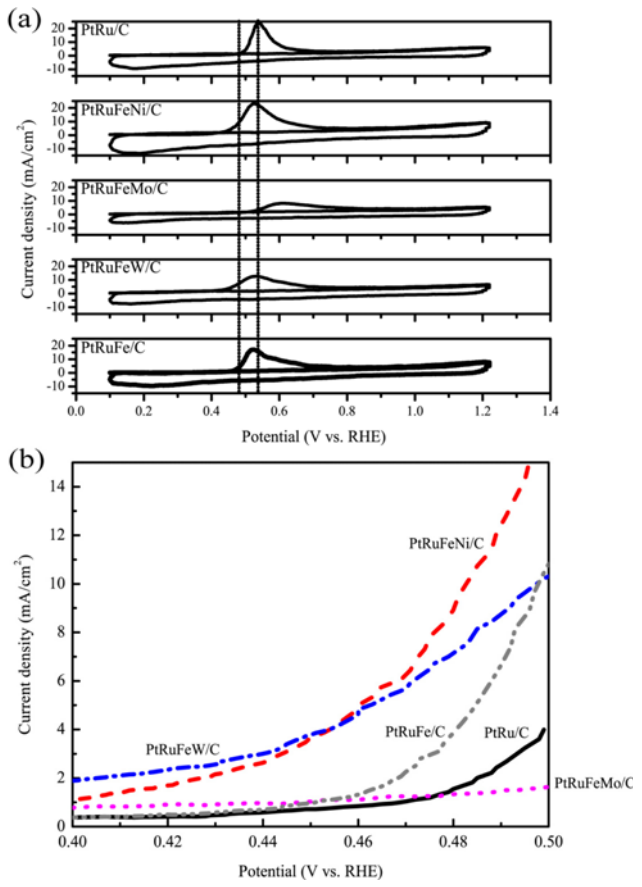

Fig. 2. (a) The CO stripping results of the PtRu/C, PtRuFeNi/C, PtRuFeMo/C, PtRuFeW/C, and PtRuFe/C [23] catalysts. An enlarged image of (a) is shown in (b) for comparison purposes.

2. Electrochemical Testing Results

The CO stripping results are shown in Fig. 2 along with the data of the PtRuFe/C catalyst [23]. In the previous study of the PtRuFe/C catalyst [23], a significantly lowered on-set potential for the CO stripping experiment was observed with respect to a PtRu/C catalyst. In the figure, it is clear that the PtRuFeNi/C and PtRuFeW/C catalysts exhibit enhanced (lowered) on-set potentials for the CO stripping experiment relative to the PtRu/C and PtRuFe/C catalysts. A closer look is shown in Fig. 2(b), and an improvement of CO_{ads} electro-oxidation reaction activity is verified for the PtRuFeNi/C and PtRuFeW/C catalysts. This result suggests that the addition of Ni or W to the Pt-Ru-Fe system can promote the CO_{ads} electro-oxidation reaction, leading to a lowered on-set potential. Unlike the Ni and W cases, noticeably suppressed performance, even worse than the binary PtRu/C catalyst, was identified in the PtRuFeMo/C catalyst. Considering that the on-set potential of a pure Pt/C catalyst is around 0.7 V [35], the on-set potential of the PtRuFeMo/C catalyst (around 0.5 V) is still superior to that of the pure platinum catalyst. In other words, the CO stripping performance of the PtRuFeMo/C catalyst is in the middle of the Pt/C and PtRu/C catalysts, meaning that Ru is not working as it does in the binary PtRu/C catalyst. As discussed in the XRD measurement section, the PtRuFeMo/C catalyst exhibited significantly low degree of alloying and it presumably contributed to the poor CO_{ads} electro-oxidation activity, but it needs further research to clarify the behavior of the PtRuFeMo/C catalyst. The electrochemical surface area (ECSA) was determined using the CO stripping area, assuming that a monolayer charge of CO_{ads} is 0.420 mC/cm^2, and the calculation results are listed in Table 2. As shown in the table, the quaternary catalysts significantly differ in the ECSA values varying from 17.4 to 35.9 m^2/g_{cat}. Note that all the catalysts exhibited similar Pt crystallite sizes of *ca.* 3.0 nm; the ECSA values suggest that a Pt-rich surface was formed in the PtRuFeNi/C and PtRuFeW/C catalysts, while a Pt-poor surface was produced in the PtRuFeMo/C catalyst. The formation of a Pt-

Table 2. The electrochemical characterization results of the commercial PtRu/C and quaternary catalysts

	ECSA (m^2/g_{cat})	Current density at 0.5 V (mA/cm^2)	Mass activity (A/g_{cat})	Specific activity (mA/m^2)
PtRu/C (E-tek)	23.7	1.16	836	35.3
PtRuFeNi/C	35.9	2.36	1700	47.4
PtRuFeMo/C	17.4	0.545	393	22.6
PtRuFeW/C	25.3	3.11	2240	88.5

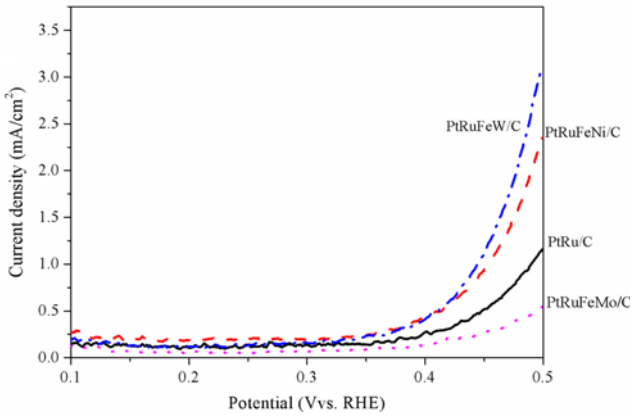

Fig. 3. The (a) LSV testing results of the PtRu/C, PtRuFeNi/C, PtRuFeMo/C, and PtRuFeW/C catalysts. The LSV testing was performed by increasing the potential from 0.1 to 0.5 V (vs. RHE) at a ramping rate of 1 mV/s. An 1 M H_2SO_4+1 M methanol solution was employed as an electrolyte solution.

rich surface is one of the key parameters that determine the MOR activity, because dehydrogenation reaction occurs on a Pt surface and CO_{ads} electro-oxidation activity is largely dependent on the surface Pt composition [36]. The ECSA values also suggest that the transition metals (Ni, Mo, and W) and/or their precursors significantly affected the surface properties of the catalysts.

The LSV test results, which were performed by increasing the applied potential from 0.1 to 0.5 V at a ramping rate of 1 mV/s, are shown in Fig. 3. It is clear that the MOR activities of the PtRuFeW/C and PtRuFeNi/C catalysts significantly outperform that of the commercial PtRu/C catalyst. On the other hand, the MOR activity of the PtRuFeMo/C catalyst is much lower than the others. Using the ECSA and current density (at 0.5 V) values, mass and specific activities were determined, and the results are listed in Table 2. As expected from the LSV results, the PtRuFeW/C catalyst exhibited the highest mass and specific activities achieving 170 and 150% improvement, respectively, with respect to the values of the commercial PtRu/C catalyst. The improvement values are even higher than the 150 and 100% of the PtRuFe/C case [23]. Although the improvement was not so impressive as the PtRuFeW/C case, the PtRuFeNi/C catalyst also exhibited a good performance leading to an increase of 100 and 34% increase in the mass and specific activities, respectively. On the other hand, a low MOR activity (only 47 and 64% of the PtRu/C catalyst for the mass and specific activities, respectively) was identified in the PtRuFeMo/C catalyst, which might have come from the high CO stripping on-set potential and Pt-poor surface formation.

3. XPS Analysis Results

The quaternary catalysts were further investigated using the XPS technique to analyze surface oxidation states. Before analyzing each component, we did a full range scan of the samples as shown in Fig. 4. The full range scan result revealed surface compositions of constituent metals which were calculated by employing XPS efficiency values for each element: 4.4 for Pt, 3.6 for Ru, 3.0 for Fe, 4.5 for Ni, 2.75 for Mo, and 2.75 for W. Based on the scan results, surface compositions of constituent metals are shown in Table 3. It is

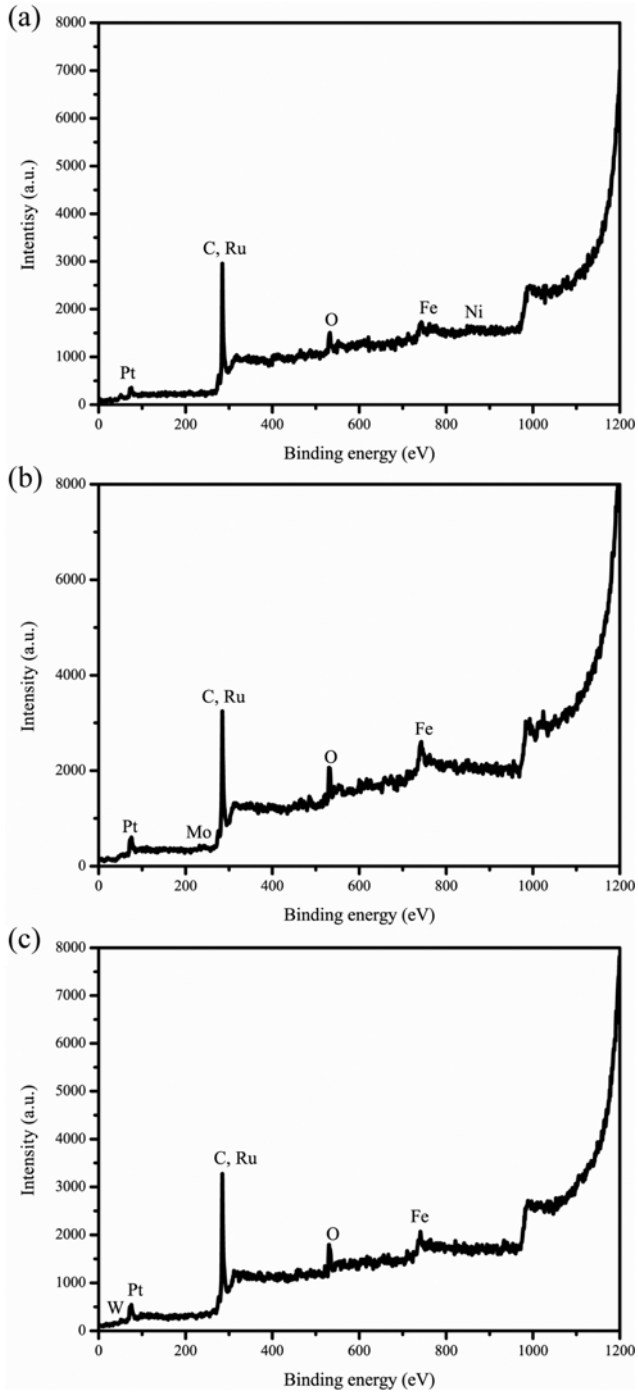

Fig. 4. The full range XPS scan results of the (a) PtRuFeNi/C, (b) PtRuFeMo/C, and (c) PtRuFeW/C catalysts.

interesting that the ratio of metals is close to initial ratio of precursors (Pt : Ru : Fe : M=40 : 20 : 20 : 20), except Mo and W which exhibited 9.9 and 11.1 at%, respectively. Here, it needs to be discussed that, according to the XPS and CO stripping experiments, high Pt surface concentration does not guarantee high ECSA values. For example, the PtRuFeNi/C catalyst exhibited the lowest surface Pt concentration of 35.5 at%, while it showed the highest ECSA value of 35.9 m^2/g_{cat}. Dispersion status of Pt on the catalyst surface might

Table 3. A summary of XPS analysis results. Ratio of the oxidation states was determined from the areas of the deconvolution results

	PtRuFeNi/C	PtRuFeMo/C	PtRuFeW/C	PtRu/C (E-tek)
Pt : Ru : Fe : M (at%)	35.5 : 22.4 : 19.5 : 22.6	41.1 : 27.3 : 21.7 : 9.9	51.5 : 21.9 : 15.5 : 11.1	81 : 19 [28]
Pt : PtO : PtO_2[a]				
Area ratio	56.1 : 22.9 : 21.0	47.8 : 30.1 : 22.1	45.9 : 37.9 : 16.2	61.5 : 23.6 : 14.9
Peak positions	71.7, 72.6, 73.7	71.5, 72.7, 74.0	71.6, 72.8, 74.1	71.8, 72.7, 73.9
Ru : RuO_xH_y : RuO_2				
Area ratio	0 : 38 : 62	0 : 25 : 75	4 : 38 : 57	6 : 62 : 31 [28]
Peak positions	N/A, 281.2, 282.3	N/A, 281.4, 282.4	280.5, 281.4, 282.4	
Fe_3O_4 : FeO : Fe_2O_3 : FeOOH				
Area ratio	1.6 : 33.8 : 26.3 : 38.3	5.2 : 29.4 : 33.3 : 32.1	1.0 : 35.6 : 28.1 : 35.3	
Peak positions	708.1, 709.7, 710.9, 712.3	708.0, 709.5, 710.8, 712.3	708.0, 709.4, 710.4, 712.2	
	Ni : NiO : $Ni(OH)_2$: NiOOH	Mo_2O_5 : MoO_3	WO_2 : WO_3	
Area ratio	8.6 : 6.8 : 47.4 : 37.2[b]	37.4 : 62.6[c]	38.2 : 61.8[d]	
Peak positions	852.8, 853.6, 855.7, 857.2	231.74, 232.6	34.6, 35.3	

[a]Determined based on Pt $4f_{7/2}$ peaks
[b]Determined based on Ni $3p_{1/2}$ peaks
[c]Determined based on Mo $3d_{3/2}$ peaks
[d]Determined based on W $4f_{7/2}$ peaks

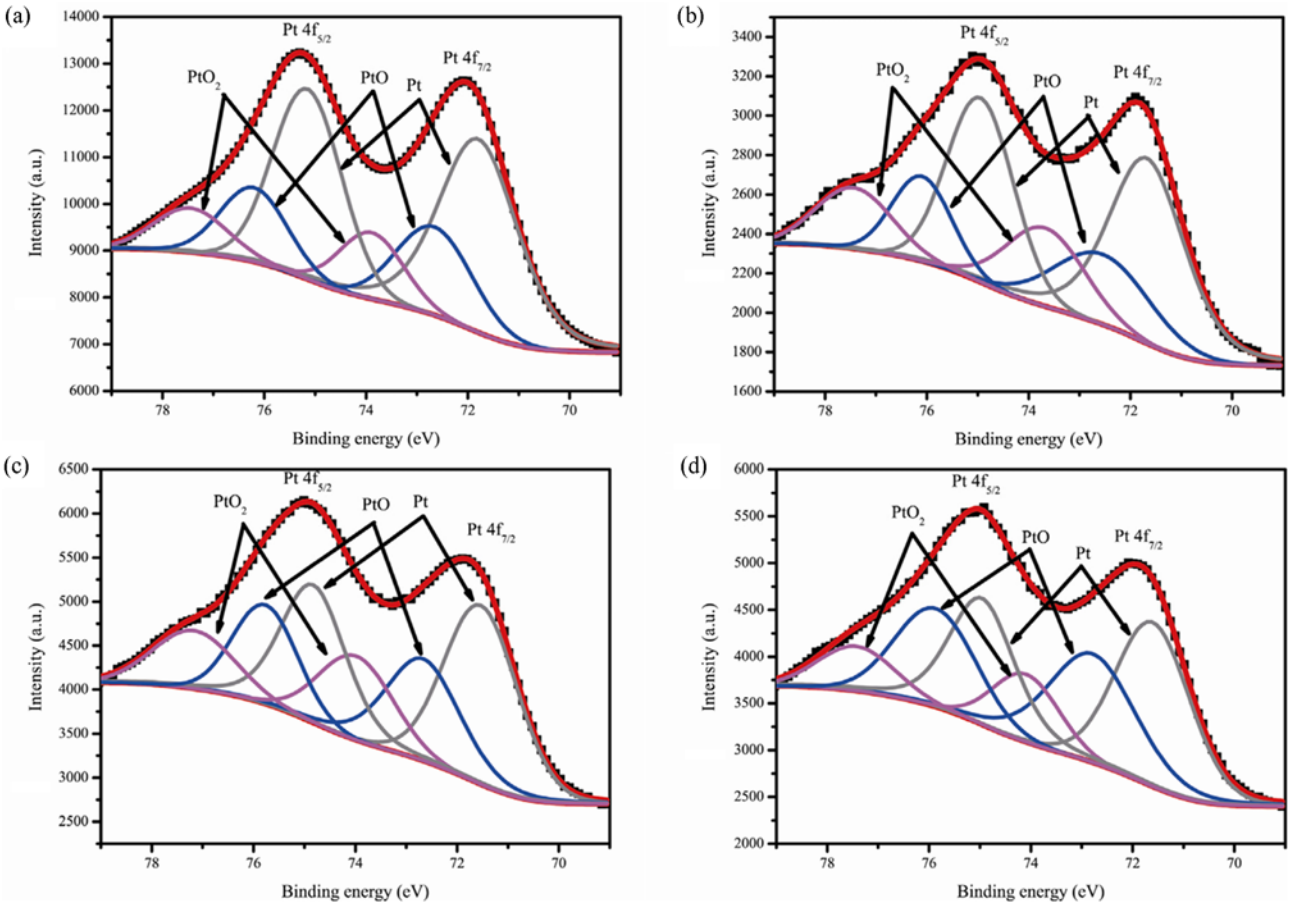

Fig. 5. The XPS measurement results of (a) PtRu/C, (b) PtRuFeNi/C, (c) PtRuFeMo/C, and (d) PtRuFeW/C catalysts for Pt $4f_{5/2}$ and $4f_{7/2}$ peaks. The deconvolution results are also denoted.

account for this gap between the XPS and ECSA results, and it is suggested that the fourth constituent of each catalyst significantly affects the surface status of the catalysts. In Fig. 4, the presence of oxygen peak should be mentioned, because it might have come from Pt oxides and, according to the XRD results, amorphous metal oxide/hydroxides of other constituent metals.

The XPS peaks of Pt $4f_{5/2}$ and $4f_{7/2}$ are shown in Fig. 5 with the results of the commercial PtRu/C catalyst. Deconvolution of the peaks was performed using the XPS peak 4.1 software [37], and the results are summarized in Table 3, including peak area ratios and peak positions. Three Pt peaks of Pt, PtO, and PtO_2 were identified in the deconvolution results, and the content of metallic Pt decreased from 61.5 in the PtRu/C catalyst to 56.1, 47.8, and 45.9 in the PtRuFeNi/C, PtRuFeMo/C, and PtRuFeW/C catalysts, respectively. On the other hand, the ratio of PtO and PtO_2 increased in the quaternary catalysts, suggesting that the addition of iron and/or fourth constituents caused a negative effect on the formation of a metallic platinum surface. The peak positions identified by the deconvolution showed negligible difference among the quaternary and the PtRu/C catalysts. It is widely accepted that an up-shift of

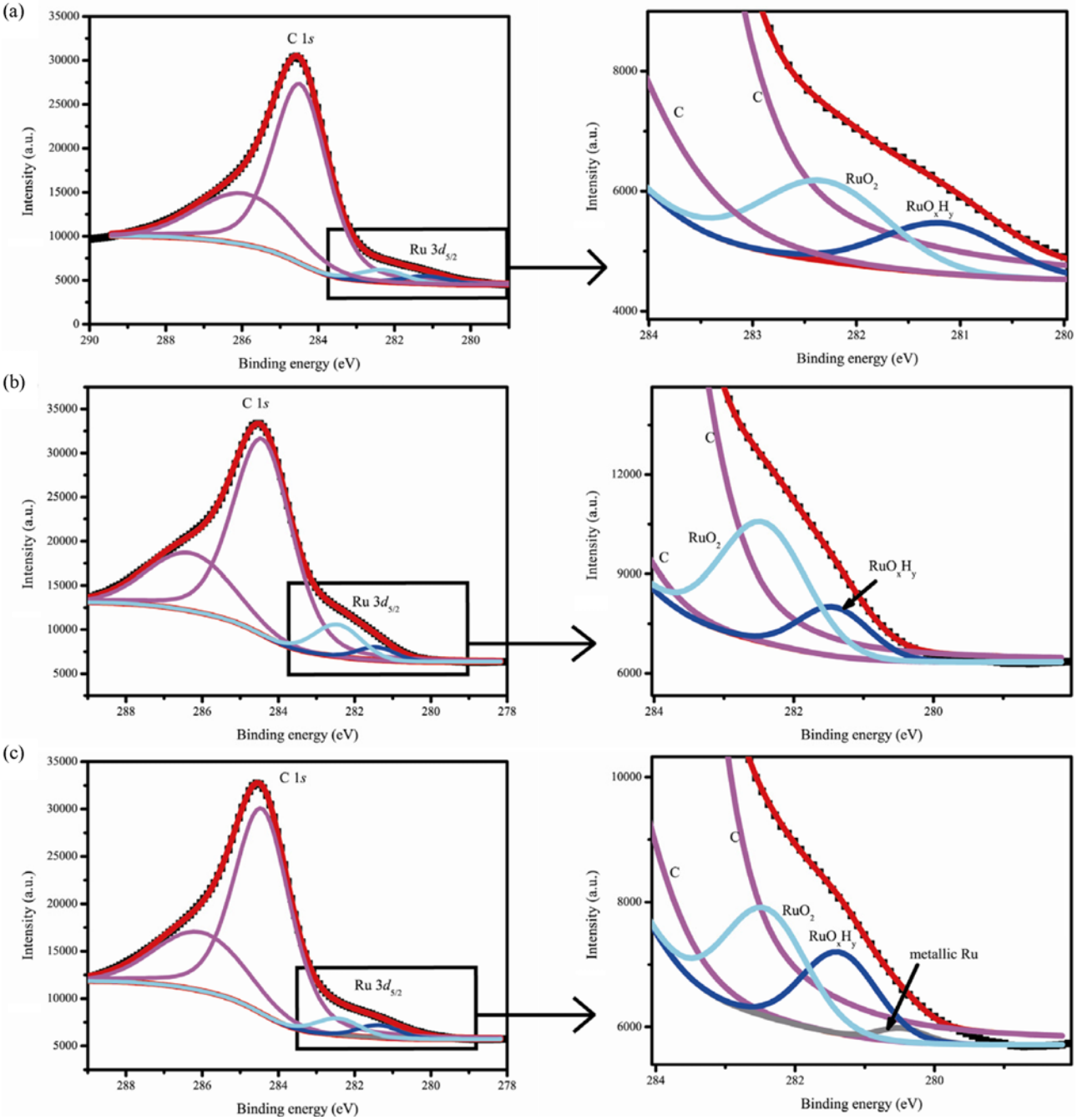

Fig. 6. The XPS measurement results of Ru $3d_{5/2}$ peaks for the (a) PtRuFeNi/C, (b) PtRuFeMo/C, and (c) PtRuFeW/C catalysts. The deconvolution results are shown in the figure.

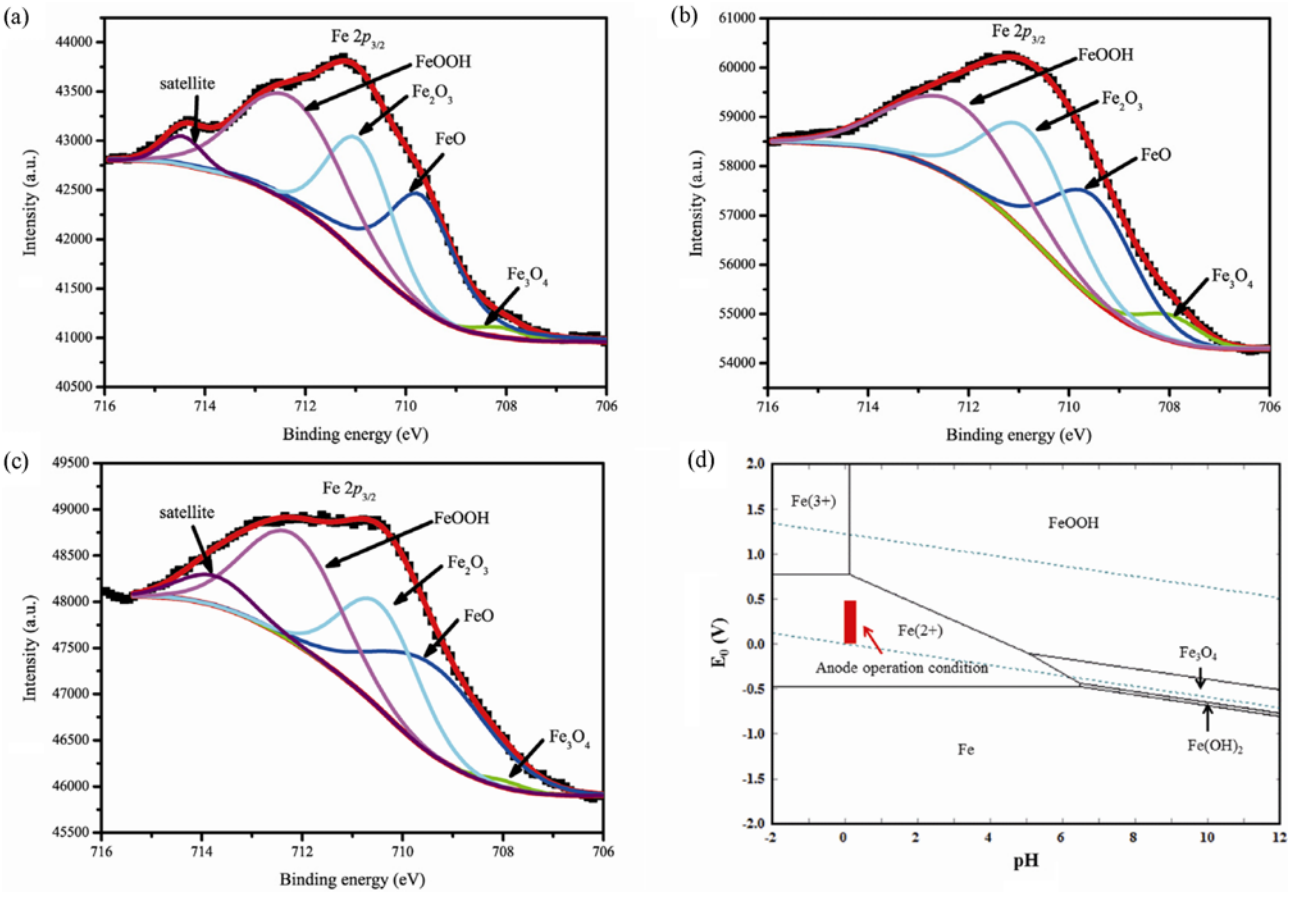

Fig. 7. The XPS measurement results of Fe $2p_{3/2}$ peak for the (a) PtRuFeNi/C, (b) PtRuFeMo/C, and (c) PtRuFeW/C catalysts. The deconvolution results are also denoted. The Pourbaix diagram of iron-water system is shown in (d).

Pt binding energy contributes to an enhanced CO oxidation activity through weakening the Pt-CO bonding, as previously shown in the PtFe catalyst [38,39]. The platinum XPS peak positions of the quaternary catalysts suggest that the electronic effect should be ruled out from a reason of the enhanced CO stripping performance, because the change in the Pt binding energies of the quaternary catalysts was negligible compared to that of the PtRu/C catalyst. Thus, it is suggested that the bi-functional mechanism is a key to account for the improved performance of the PtRuFeNi/C and PtRuFeW/C catalysts.

Fig. 6 shows the XPS spectra of Ru $3d_{5/2}$ peaks of the quaternary catalysts. A deconvolution calculation was performed to separate the Ru peaks from those of C 1s and detailed results are listed in Table 3. As noted in the figure, RuO_xH_y and RuO_2 peaks were observed in all of the quaternary catalysts, while metallic Ru was identified only in the PtRuFeW/C catalyst. Among the three types of Ru, RuO_xH_y is the most active form for the MOR followed by metallic Ru [31], while RuO_2, which was identified as a dominant phase in the quaternary catalysts, is known as a poor promoter for the MOR [32,40,41]. The XPS results revealed that the PtRuFeMo/C catalyst exhibited highest ratio of RuO_2 (75 at%) which might have contributed to the poor CO_{ads} and methanol electro-oxidation reactions.

The XPS spectra of the third constituent, iron, are shown in Fig. 7(a)-(c). Four oxidation states of Fe_3O_4, FeO, Fe_2O_3, and FeOOH were identified through deconvolution calculations, and the results are summarized in Table 3. Significant changes were not observed in the ratio of the four oxidation states, resulting in FeO, Fe_2O_3, and FeOOH as major oxidation states of iron in the quaternary catalysts. Peak positions of Fe_3O_4, FeO, Fe_2O_3 were close to reference data, while a noticeable up-shift was observed in the peaks of FeOOH. Note that the peak position of FeOOH is known to be near 711.2 eV, while it was observed around 712.3 eV in the quaternary catalysts. As the peak positions of Pt and Ru components were close to reference positions, it is reasonable to suspect that FeOOH might exist in a different form, which is not clear in the current stage. Pourbaix diagram of iron-water system was calculated using the HSC chemistry code [42] to account for the catalyst role of iron compounds, and the result is shown in Fig. 7(d). As shown in the figure, Fe(2+) is the most stable state of iron in the DMFC anode condition, suggesting following equations as a feasible role of iron for the improved MOR and CO_{ads} electro-oxidation activities. Here, the role of iron oxides/hydroxides needs further research to clarify the reaction mechanism.

$$Pt+CH_3OH \rightarrow Pt\text{-}CO+4H^++4e^- \quad (6)$$

$$Pt+FeO+H_2O \rightarrow Pt\text{-}H+FeOOH \quad (7)$$

$$Pt\text{-}CO+FeOOH \rightarrow Pt+FeO+H_2O+H^++e^- \quad (8)$$

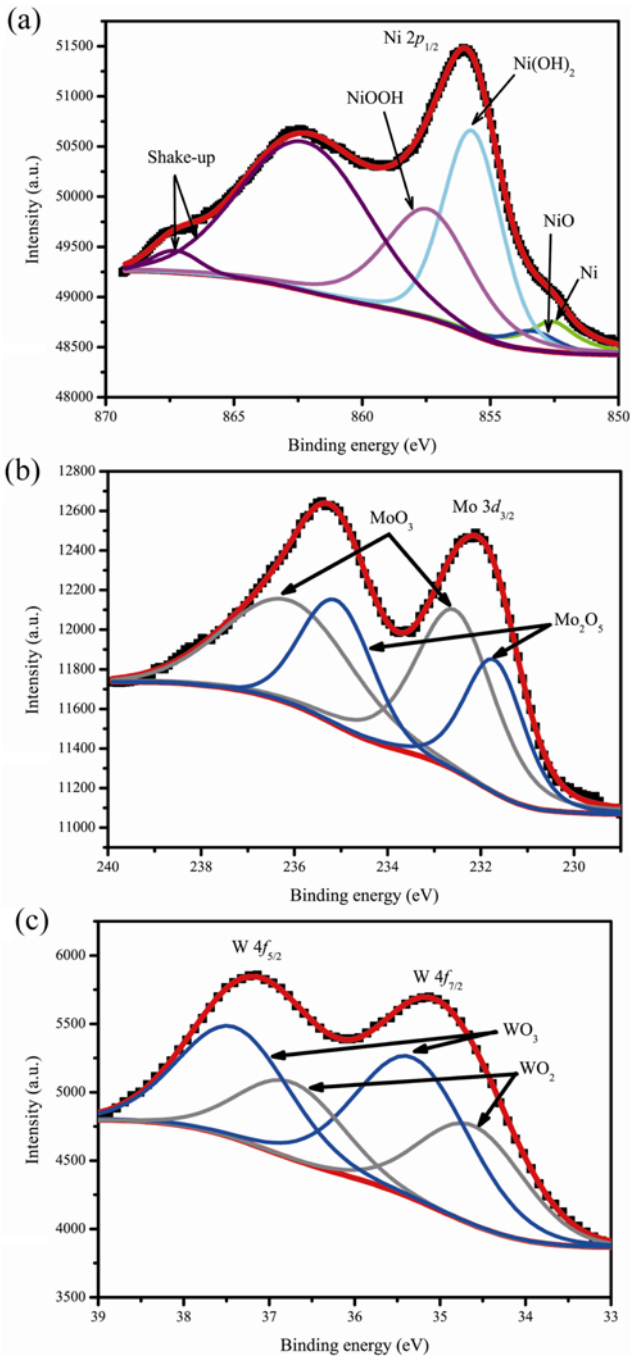

Fig. 8. The XPS measurement results of (a) Ni 2p for the PtRuFeNi/C catalyst, (b) Mo 3d for the PtRuFeMo/C catalyst, and (c) W 4f for the PtRuFeW/C catalyst. The deconvolution results are also included.

The XPS spectra of the fourth component, Ni, W, and Mo, are shown in Fig. 8. The peaks of Ni $2p_{3/2}$ and Ni $2p_{1/2}$ are shown in Fig. 8(a), including deconvolution results for the Ni $2p_{3/2}$ peaks. The deconvolution was performed following a previous report [43]: starting peak positions were 852.7, 853.8, 855.6, and 857.3 eV for Ni, NiO, $Ni(OH)_2$, and NiOOH, respectively. Detailed results of the deconvolution calculations are listed in Table 3, and it was revealed that peak positions of Ni, NiO, $Ni(OH)_2$, and NiOOH were 852.8, 853.6, 855.7, and 857.2 eV, respectively, meaning that a noticeable peak shift was not induced by other atoms. The deconvolution results revealed that major components of Ni are $Ni(OH)_2$ and NiOOH, which are known to have an activity for the MOR [43]. But, in the presence of platinum, the following reaction scheme suggested by Park et al. [44] might account for the improved performance of the PtRuFeNi/C catalyst for the MOR and CO stripping reactions.

$$NiOOH+Pt\text{-}H \rightarrow Ni(OH)_2+Pt \quad (9)$$

$$Ni(OH)_2 \rightarrow NiOOH+H^+ + e^- \quad (10)$$

Here, hydrogen spill-over occurs from Pt surface to NiOOH to produce $Ni(OH)_2$ and fresh Pt surface which is ready for a next reaction (Eq. (9)). And then $Ni(OH)_2$ is decomposed into NiOOH to produce proton and electron as shown in Eq. (10).

The XPS results measured for Mo $3d_{5/2}$ binding energies are shown in Fig. 8(b). No signs of Mo and MoO_2 were observed, while MoO_3 (at 232.6 and 236.0 eV) and Mo_2O_5 (231.7 and 235.1 eV) were identified as the major components of Mo [45]. Deconvolution results are also shown in the figure and detailed information is provided in Table 3. Previously, binary Pt-MoO_x and PtMo catalysts were investigated by other groups and enhanced CO oxidation activity was observed [22,46,47], while it was also revealed that Pt-MoO_x/C catalyst exhibited poor MOR activity [48]. In the case of a ternary PtRuMo catalyst, an excellent MOR activity was reported by Lima et al. [12] although some researchers published the opposite results [49,50]. These contradictory results mean that a systematic investigation should be done to understand the role of Mo, including the effects of precursors, degree of alloying, and oxidation states of Mo. But, in the present study, it is clear that the molybdenum oxides formed in the PtRuFeMo/C catalyst seldom played a positive role for the MOR and CO stripping reactions. A low degree of alloying value might account for the low MOR and CO stripping activities, but it is not clear yet.

Fig. 8(c) shows the XPS peaks of W $4f_{5/2}$ and $4f_{7/2}$ observed from the PtRuFeW/C catalyst. WO_2 and WO_3 peaks were identified as major components, while no signs of metallic tungsten were found. The deconvolution results for the WO_2 and WO_3 peaks are listed in Table 3. Note that the peak position of WO_2 (34.6 eV, W $4f_{7/2}$) is somewhat different from the reference data (32.4 eV), meaning that the peak assigned as WO_2 might come from substoichiometric tungsten oxides (WO_{3-x}) or tungsten bronze (H_yWO_3) [51,52]. It is known that these forms of tungsten play a positive role for the MOR through spillover of hydrogen from the Pt to WO_x leading to an enhanced dehydrogenation reaction as follows [51,52]:

$$Pt\text{-}H+WO_x \rightarrow Pt+H\text{-}WO_x \quad (11)$$

In addition, Micoud et al. [52] observed CO oxidation at 0.1 V using a Pt/WO_x catalyst, which can be explained by support of WO_x through the bi-functional mechanism, because Pt requires higher potential (above 0.6 V) to produce oxygenated species. In other words, WO_x can produce oxygenated species even at 0.1 V to react with CO adsorbed on Pt surface. In the PtRuFeW/C catalyst, high MOR activity and low on-set potential for the CO stripping reaction were observed, and the role of WO_x species introduced in the previous results [51,52] well accounts for the positive effect of W incorporation.

CONCLUSIONS

Structural and electrochemical properties of three quaternary electrocatalysts of PtRuFeNi/C, PtRuFeMo/C, and PtRuFeW/C were investigated for the MOR. Significantly enhanced CO_{ads} electrooxidation activities were observed in the PtRuFeNi/C and PtRuFeW/C catalysts, while the PtRuFeMo/C catalyst exhibited a suppressed performance. For the MOR, the PtRuFeNi/C and PtRuFeW/C catalysts significantly outperformed the commercial PtRu/C catalyst; The LSV testing results revealed that the MOR activity of the PtRuFeW/C catalyst exceeds the mass and specific activities of the PtRu/C catalyst by 170 and 150%, respectively. According to the XRD measurement results, the incorporation of Ni, Mo, and W can significantly change the degree of alloying which varied from 0.084 to 0.237. The XRD and XPS results also showed that actual forms of the synthesized catalysts were close to a nano-composite of Pt-alloy and amorphous metal oxides/hydroxides, leading to a conclusion that the bi-functional mechanism played a dominant role for the improved MOR and CO stripping activities.

ACKNOWLEDGEMENT

This work was sponsored by the Nuclear R&D program of the Korean Ministry of Science, ICT & Future Planning (No. 2012M2A8A5025802).

REFERENCES

1. A. S. Arico, S. Srinivasan and V. Antonucci, *Fuel Cells*, **1**, 133 (2001).
2. M. Watanabe and S. Motoo, *J. Electroanal. Chem.*, **229**, 395 (1987).
3. N. M. Markovic, H. A. Gasteiger and P. N. Ross Jr., *Electrochim. Acta*, **40**, 91 (1995).
4. W. Chrzanowski and A. Wieckowski, *Langmuir*, **14**, 1967 (1998).
5. O. A. Petrii, *J. Solid State Electrochem.*, **12**, 609 (2008).
6. J. H. Choi, K. W. Park, B. K. Kwon and Y. E. Sung, *J. Electrochem. Soc.*, **150**, A973 (2003).
7. Z. B. Wang, G. P. Yin, P. F. Shi and Y. C. Sun, *Electrochem. Solid-State Lett.*, **9**, A13 (2006).
8. J. Liu, J. Cao, Q. Huang, X. Li, Z. Zou and H. Yang, *J. Power Sources*, **175**, 159 (2008).
9. V. A. Ribeiro, O. V. Correa, A. O. Neto, M. Linardi and E. V. Spinace, *Appl. Catal. A: Gen.*, **372**, 162 (2010).
10. M. K. Jeon, K. R. Lee, H. Daimon, A. Nakahara and S. I. Woo, *Catal. Today*, **132**, 123 (2008).
11. J. S. Cooper and P. J. McGinn, *J. Power Sources*, **163**, 330 (2006).
12. A. Lima, C. Coutanceau, J. M. Léger and C. Lamy, *J. Appl. Electrochem.*, **31**, 379 (2001).
13. M. Umeda, H. Ojima, M. Mohamedi and I. Uchida, *J. Power Sources*, **136**, 10 (2004).
14. M. Goetz and H. Wendt, *J. Appl. Electrochem.*, **31**, 811 (2001).
15. C. Roth, M. Goetz and H. Fuess, *J. Appl. Electrochem.*, **31**, 793 (2001).
16. E. Antolini, *Appl. Catal. B: Environ.*, **74**, 324 (2007).
17. C. Lamy, A. Lima, V. LeRhun, F. Delime, C. Coutanceau and J. M. Léger, *J. Power Sources*, **105**, 283 (2002).
18. U. M. Demirci, *J. Power Sources*, **173**, 11 (2007).
19. T. R. Ralph and M. P. Hogarth, *Platin. Met. Rev.*, **46**, 3 (2002).
20. R. C. Urian, A. F. Gullá and S. Mukerjee, *J. Electroanal. Chem.*, **554**, 307 (2003).
21. P. P. Lopes, K. S. Feitas and E. A. Ticianelli, *Electrocatal.*, **1**, 200 (2010).
22. S. M. M. Ehteshami and S. H. Chan, *Electrochim. Acta*, **93**, 334 (2013).
23. M. K. Jeon, J. Y. Won, K. R. Lee and S. I. Woo, *Electrochem. Commun.*, **9**, 2163 (2007).
24. K. R. Lee, M. K. Jeon and S. I. Woo, *Appl. Catal. B: Environ.*, **91**, 428 (2009).
25. T. J. Schmidt, H. A. Gasteiger, G. D. Stäb, P. M. Urban, D. M. Kolb and R. J. Behm, *J. Electrochem. Soc.*, **145**, 2354 (1998).
26. E. Antolini and F. Cardellini, *J. Alloys Compd.*, **315**, 118 (2001).
27. K. Watanabe, *Trans. Jpn. Inst. Met.*, **29**, 80 (1988).
28. C. Leroux, M. C. Cadeville, V. Pierron-Bohnes, G. Inden and F. Hinz, *J. Phys. F: Met. Phys.*, **18**, 2033 (1988).
29. E. Raub and W. Mahler, *Z. Metallkd.*, **46**, 210 (1955).
30. H. L. Luo, *J. Less Common Met.*, **156**, 299 (1968).
31. D. R. Rolison, P. L. Hagans, K. E. Swider and J. W. Long, *Langmuir*, **15**, 774 (1999).
32. J. W. Long, R. M. Stroud, K. E. Swider-Lyons and D. R. Rolison, *J. Phys. Chem. B*, **104**, 9772 (2000).
33. M. K. Jeon, K. R. Lee, H. J. Jeon and S. I. Woo, *J. Appl. Electrochem.*, **39**, 1503 (2009).
34. C. He, H. R. Kunz and J. M. Fenton, *J. Electrochem. Soc.*, **144**, 970 (1997).
35. M. K. Jeon, H. Daimon, K. R. Lee, A. Nakahara and S. I. Woo, *Electrochem. Commun.*, **9**, 2692 (2007).
36. G. A. Camara, M. J. Giz, V. A. Paganin and E. A. Ticianelli, *J. Electroanal. Chem.*, **537**, 21 (2002).
37. R. W. M. Kwok, *XPS peak fitting program for WIN95/98 XPSPEAK version 4.1*, Department of Chemistry, The Chinese University of Hong Kong, Shatin, Hong Kong (2000).
38. M. Watanabe, H. Igarashi and T. Fujino, *Electrochem.*, **6**, 1194 (1999).
39. M. Watanabe, Y. Zhu and H. Uchida, *J. Phys. Chem. B*, **104**, 1762 (2000).
40. M. K. Jeon, J. Y. Won and S. I. Woo, *Electrochem. Solid-State Lett.*, **10**, B23 (2007).
41. B. J. Kennedy and A. W. Smith, *J. Electroanal. Chem.*, **293**, 103 (1990).
42. A. Roine, *Outokumpu HSC chemistry for windows*, Pori, Finland (2002).
43. R. Manoharan and G. B. Goodenough, *J. Mater. Chem.*, **2**, 875 (1992).
44. K. W. Park, J. H. Choi, B. K. Kwon, S. A. Lee, Y. E. Sung, H. Y. Ha, S. A. Hong, H. Kim and A. Wieckowski, *J. Phys. Chem. B*, **106**, 1869 (2002).
45. N. Tsiouvaras, M. A. Peña, J. L. G. Fierro, E. Pastor and M. V. Martínez-Huerta, *Catal. Today*, **158**, 12 (2010).
46. T. Ioroi, K. Yasuda, Z. Siroma, N. Fujiwara and Y. Miyazaki, *J. Electrochem. Soc.*, **150**, A1225 (2003).
47. Z. Liu, J. E. Hu, Q. Wang, K. Gaskell, A. I. Frenkel, G. S. Jackson and B. Eichhorn, *J. Am. Chem. Soc.*, **131**, 6924 (2009).
48. L. Ma, X. Zhao, F. Si, C. Liu, J. Liao, L. Liang and W. Xing, *Electro-*

chim. Acta, **55**, 9105 (2010).
49. E. Teliz, V. Díaz, I. Pérez, M. Corengia and C. F. Zinola, *Int. J. Hydrogen Energy*, **37**, 14761 (2012).
50. M. K. Jeon, K. R. Lee and S. I. Woo, *Korean J. Chem. Eng.*, **26**, 1028 (2009).
51. Z. B. Wang, P. J. Zuo and G. P. Yin, *J. Alloys Compd.*, **479**, 395 (2009).
52. F. Micoud, F. Maillard, A. Bonnefont, N. Job and M. Chatenet, *Phys. Chem. Chem. Phys.*, **12**, 1182 (2010).